OFDM MIMO Radar for Low-Grazing Angle Tracking †

Satyabrata Sen and Arye Nehorai
Department of Electrical and Systems Engineering
Washington University in St. Louis
One Brookings Drive, St. Louis, MO 63130, USA
Email: {ssen3, nehorai}@ese.wustl.edu
Phone: 314-935-7520 Fax: 314-935-7500

***Abstract*—We develop a low-grazing angle (LGA) tracking method considering realistic physical and statistical effects, such as earth's curvature, vertical refractivity gradient of standard lower atmosphere, and non-Gaussian characteristics of sea-clutter. We employ a co-located multiple-input-multiple-output (MIMO) radar configuration using wideband orthogonal frequency division multiplexing (OFDM) signalling scheme. Apart from the frequency diversity provided by OFDM, we also exploit polarization to resolve the multipath signals by using polarization-sensitive transceivers. Thus, we can track the scattering coefficients of the target at different frequencies along with its position and velocity. We apply a sequential Monte Carlo method (particle filter) to track the target. Our numerical examples demonstrate the achieved performance improvements due to realistic physical modeling and OFDM MIMO configuration.**

I. Introduction

Tracking targets in a low-grazing angle scenario (LGA) [1]-[4] is one of the most challenging problems in radar. To develop an accurate tracking method it is important that we incorporate the underlying physical phenomena. In the low-grazing angle scenario, the radar measurements are affected by many factors [5]-[7], such as the ever-changing meteorological conditions in the troposphere (the lowest portion of earth's atmosphere), earth's curved surface, roughness of the sea-surface, etc. Therefore, the challenge is to consider these complex physical behaviors as realistically as possible, yet keep the model amenable to signal processing. In this work, we consider the effects of earth's curvature and linear refractivity gradient of the horizontally stratified atmosphere [5], [8] while modeling the specular multipath signals. The randomly reflected returns (clutter) are statistically modeled as a compound-Gaussian process [9], [10].

Furthermore, to resolve the specular multipath components it is generally known to use short pulse, multi-carrier wideband radar signals [1], [11], [12]. So, we employ the orthogonal frequency division multiplexing (OFDM) scheme [13], which is one of the ways to accomplish simultaneous use of several sub-carriers. The frequency diversity of OFDM also provides richer information about the target as different scattering centers resonate at different frequencies. To achieve such waveform diversity we employ a co-located multiple-input-multiple-output (MIMO) radar configuration [14]. Additionally, in [15], [16] we have shown that polarization allows identification of correlated source signals (e.g., multipath) with small separation angles. Hence, we consider polarization-sensitive transceivers in our work.

In Section II, we first describe the effects of the curvature of earth and variation of the refractive index on LGA propagation. Then, in Section III, we develop a target dynamic state model and a parametric OFDM MIMO radar measurement model. Based on these models, in Section IV we present a sequential Monte Carlo approach for target tracking. Numerical examples and conclusions are presented in Sections V and VI, respectively.

II. Effects of Tropospheric Propagation

To formulate a realistic model of the LGA propagation, we consider the curvature of earth and bending of the signal path due to the refraction in the troposphere. We assume a horizontally stratified atmosphere in which the refractive index decreases nearly linearly with height at low altitudes, but does not vary horizontally along the surface of earth [5], [8]. This assumption is based on the fact that the atmosphere is horizontally much less variable than vertically, in particular over ocean surfaces [7]. In such scenarios, a ray propagating over the true earth of radius a can be equivalently represented over a flat earth with effective radius [5]

$$a_{\mathrm{e}} = a\left(1 + a\frac{dN}{dh}10^{-6}\right)^{-1}, \tag{1}$$

where h denotes the height above earth's surface and N is the refractivity, defined as $N = 10^6(n-1)$ (N-units). Here n is the refractive index, which is related to the dielectric constant ϵ_{r} as $n = \epsilon_{\mathrm{r}}^2$. In normal or standard atmosphere, because of the decrease in pressure, humidity, and temperature with height above ground, the refractivity gradient is considered to be $dN/dh = -39$ N-units/km [6], [7]. This makes a ray to refract downward toward earth's surface, but with a curvature less than earth's radius [7].

To incorporate these effects into our model, let us consider two points at heights h and z and separated from each other

† This work was supported by the ONR Grant N000140810849 and the Department of Defense under the Air Force Office of Scientific Research MURI Grant FA9550-05-1-0443.

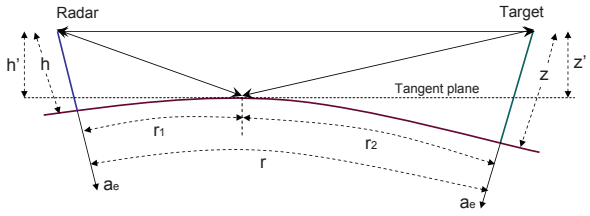

Fig. 1. Equivalent representations between curved and flat earths.

by distance r (see Fig. 1). Then, we can write an equivalent version of the modified heights over the flat-earth model as [17]

$$h' \simeq h - \frac{(r-r_1)^2}{2a_{\mathrm{e}}}, \tag{2}$$

$$z' \simeq z - \frac{r_1^2}{2a_{\mathrm{e}}}, \tag{3}$$

where the point of reflection r_1 is evaluated by solving the following cubic equation [5]

$$2r_1^3 - 3rr_1^2 + \left[r^2 - 2a_{\mathrm{e}}(h+z)\right] r_1 + 2a_{\mathrm{e}} zr = 0.$$

III. State and Measurement Models

In this section, we first present a dynamic state model for target tracking. Then, we develop an OFDM MIMO radar signal model that accounts for polarimetric measurements over multiple frequencies.

A. Dynamic State Model

We consider the position, velocity, and scattering parameters at different frequencies of the target into our state model. The scattering matrix of the target at a particular frequency can be represented as

$$\boldsymbol{S}_l^{\mathrm{t}} = \begin{bmatrix} s_l^{\mathrm{hh}} & s_l^{\mathrm{hv}} \\ s_l^{\mathrm{vh}} & s_l^{\mathrm{vv}} \end{bmatrix}, \tag{4}$$

where s_l^{hv} is the complex scattering coefficient of the target in the horizontally polarized component of the received signal due to the vertically polarized component of the transmitted signal at the l-th frequency; similarly for the other quantities. From Huynen's work [18], we also know that $\boldsymbol{S}_l^{\mathrm{t}} \triangleq \boldsymbol{U}_l^* \boldsymbol{D}_l \boldsymbol{U}_l^H$ where

- $\boldsymbol{U}_l$ is a unitary matrix

$$\boldsymbol{U}_l = \begin{bmatrix} \cos\vartheta_l & -\sin\vartheta_l \\ \sin\vartheta_l & \cos\vartheta_l \end{bmatrix} \begin{bmatrix} \cos\varepsilon_l & j\sin\varepsilon_l \\ j\sin\varepsilon_l & \cos\varepsilon_l \end{bmatrix}, \tag{5}$$

  where ϑ_l is the orientation angle of the target ellipse with respect to line of sight and relative to the radar $(-90^\circ \le \vartheta_l \le 90^\circ)$; ε_l is the ellipticity of the target $(-45^\circ \le \varepsilon_l \le 45^\circ)$ [19].
- $\boldsymbol{D}_l$ is a diagonal matrix

$$\boldsymbol{D}_l = m_l\, e^{j\varrho_l} \begin{bmatrix} e^{j\varsigma_l} & 0 \\ 0 & e^{-j\varsigma_l}\tan^2\varpi_l \end{bmatrix}, \tag{6}$$

  where m_l is the maximum target amplitude; ϱ_l is the absolute phase of the scattering matrix $(-180^\circ \le \varrho_l \le 180^\circ)$; ς_l is called the target skip angle $(-45^\circ \le \varsigma_l \le 45^\circ)$; ϖ_l is called the target characteristic angle $(0^\circ \le \varpi_l \le 45^\circ)$ [19].

In general, all of these six target variables ϑ_l, ε_l, m_l, ϱ_l, ς_l, and ϖ_l are functions of frequency and aspect direction [18].

Considering a target at position $(x,\ y,\ z)$ and moving with velocity $\boldsymbol{v}(= \dot{x}\hat{i} + \dot{y}\hat{j} + \dot{z}\hat{k})$, we construct the state vector as follows:

$$\boldsymbol{x} = \left[x, y, z, \dot{x}, \dot{y}, \dot{z}, \boldsymbol{\vartheta}^T, \boldsymbol{\varepsilon}^T, \boldsymbol{m}^T, \boldsymbol{\varrho}^T, \boldsymbol{\varsigma}^T, \boldsymbol{\varpi}^T\right]^T, \tag{7}$$

where $\boldsymbol{\vartheta} = [\vartheta_1, \ldots, \vartheta_{_L}]^T$, $\boldsymbol{\varepsilon} = [\varepsilon_1, \ldots, \varepsilon_{_L}]^T$, $\boldsymbol{m} = [m_1, \ldots, m_{_L}]^T$, $\boldsymbol{\varrho} = [\varrho_1, \ldots, \varrho_{_L}]^T$, $\boldsymbol{\varsigma} = [\varsigma_1, \ldots, \varsigma_{_L}]^T$, and $\boldsymbol{\varpi} = [\varpi_1, \ldots, \varpi_{_L}]^T$.

Assuming constant velocity movement, we obtain a linear dynamic state equation at k-th time step as

$$\boldsymbol{x}_k = \begin{bmatrix} \begin{bmatrix} \boldsymbol{I}_3 & T_{\mathrm{PRI}}\boldsymbol{I}_3 \\ \boldsymbol{0} & \boldsymbol{I}_3 \end{bmatrix} & \boldsymbol{0} \\ \boldsymbol{0} & \boldsymbol{I}_{6L} \end{bmatrix} \boldsymbol{x}_{k-1} + \boldsymbol{w}_k, \tag{8}$$

where T_{PRI} denotes the pulse repetition interval (PRI) and $\boldsymbol{w}$ represents the state noise. In this model, we consider that the scattering coefficients of the target are almost constant. This is true, for example, when the target is far away from the radar. We assume $\boldsymbol{w}$ to be zero-mean Gaussian distributed random vector with covariance matrix

$$\boldsymbol{\Sigma}_{\boldsymbol{w}} = \begin{bmatrix} q_{\mathrm{pv}} \begin{bmatrix} \frac{T_{\mathrm{PRI}}^4}{3}\boldsymbol{I}_3 & \frac{T_{\mathrm{PRI}}^3}{2}\boldsymbol{I}_3 \\ \frac{T_{\mathrm{PRI}}^3}{2}\boldsymbol{I}_3 & T_{\mathrm{PRI}}^2\boldsymbol{I}_3 \end{bmatrix} & \boldsymbol{0} \\ \boldsymbol{0} & q_{\mathrm{scat}}\boldsymbol{I}_{6L} \end{bmatrix},$$

where q_{pv} and q_{scat} are constants. Hence, the position and velocity of the target are statistically independent of the scattering coefficients.

B. Measurement Model

We consider an array of L transceivers forming an $L \times L$ co-located MIMO configuration. Each of the transceivers is positioned at $(0, 0, h_l)$, $l = 0, 1, \ldots, L-1$, and transmits with a carrier frequency f_l forming an OFDM signalling system with $\Delta f = B/(L+1) = 1/T$, where B is the total bandwidth and T denotes pulse duration. Each of the transceivers is capable of transmitting and receiving polarized signals. We formulate the complex envelope of the signal at the j-th receiver due to the i-th transmitter as a summation of three terms

$$\begin{aligned} \boldsymbol{y}_{ij}(t, \boldsymbol{x}_k) &= \boldsymbol{\mu}_{ij}(t, \boldsymbol{x}_k) + \boldsymbol{c}_{ij}(t) + \boldsymbol{e}_{ij}(t), \\ &\quad \text{for } i, j = 0, \ldots, L-1,\ t = 0, \ldots, N-1, \end{aligned} \tag{9}$$

where $\boldsymbol{\mu}_{ij}(t, \boldsymbol{x}_k)$ represents the signal part of the measurement, composed of the coherent sum of direct and specularly reflected signals (as shown in Fig. 2), and it depends on the target state vector $\boldsymbol{x}_k$; $\boldsymbol{c}_{ij}(t)$ represents the clutter, comprising of any randomly reflected returns within the time-span of interest; $\boldsymbol{e}_{ij}(t)$ is the thermal noise.

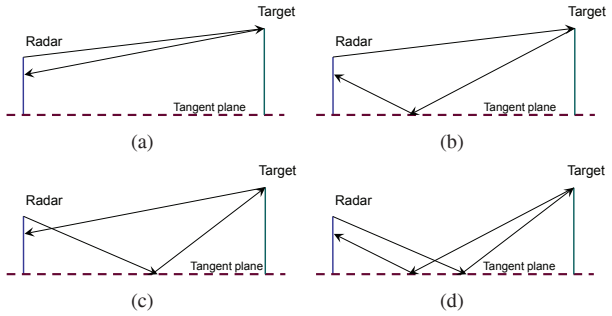

Fig. 2. (a) Direct-direct, (b) direct-reflected, (c) reflected-direct, and (b) reflected-reflected signal paths.

The complex envelope of $\boldsymbol{\mu}_{ij}(t,\boldsymbol{x}_k)$ can be represented as

$$\boldsymbol{\mu}_{ij}(t,\boldsymbol{x}_k) = \boldsymbol{\mu}_{ij}^{\mathrm{dd}}(t) + \boldsymbol{\mu}_{ij}^{\mathrm{dr}}(t) + \boldsymbol{\mu}_{ij}^{\mathrm{rd}}(t) + \boldsymbol{\mu}_{ij}^{\mathrm{rr}}(t), \qquad (10)$$

where

$$\begin{aligned}
\boldsymbol{\mu}_{ij}^{\mathrm{dd}}(t) &= \boldsymbol{V}(\theta_j^{\mathrm{d}},\phi)\boldsymbol{S}_i\boldsymbol{\xi}\left(\tau_{ij}^{\mathrm{dd}}, f_{\mathrm{D}ij}^{\mathrm{dd}}\right),\\
\boldsymbol{\mu}_{ij}^{\mathrm{dr}}(t) &= \boldsymbol{V}(\theta_j^{\mathrm{r}},\phi)\boldsymbol{\Gamma}_j\boldsymbol{S}_i\boldsymbol{\xi}\left(\tau_{ij}^{\mathrm{dr}}, f_{\mathrm{D}ij}^{\mathrm{dr}}\right),\\
\boldsymbol{\mu}_{ij}^{\mathrm{rd}}(t) &= \boldsymbol{V}(\theta_j^{\mathrm{d}},\phi)\boldsymbol{S}_i\boldsymbol{\Gamma}_i\boldsymbol{\xi}\left(\tau_{ij}^{\mathrm{rd}}, f_{\mathrm{D}ij}^{\mathrm{rd}}\right),\\
\boldsymbol{\mu}_{ij}^{\mathrm{rr}}(t) &= \boldsymbol{V}(\theta_j^{\mathrm{r}},\phi)\boldsymbol{\Gamma}_j\boldsymbol{S}_i\boldsymbol{\Gamma}_i\boldsymbol{\xi}\left(\tau_{ij}^{\mathrm{rr}}, f_{\mathrm{D}ij}^{\mathrm{rr}}\right),
\end{aligned}$$

with

$$\boldsymbol{\xi}\left(\tau, f_{\mathrm{D}}\right) \triangleq \boldsymbol{p}(\alpha_i,\beta_i)a_i e^{-j2\pi(f_i+f_{\mathrm{D}})\tau}e^{j2\pi f_{\mathrm{D}}t}, \qquad (11)$$

and

- $\phi = \arctan(y/x)$, $\theta_j^{\mathrm{d}} = \arctan\left((z-h_j)/\sqrt{x^2+y^2}\right)$, $\theta_j^{\mathrm{r}} = \arctan\left((z+h_j)/\sqrt{x^2+y^2}\right)$.
- $\boldsymbol{V}(\theta,\phi)$ denotes the array factor for a two-dimensional polarimetric sensor, defined as

$$\boldsymbol{V}(\theta,\phi) = \begin{bmatrix} -\sin\phi & -\cos\phi\sin\theta \\ 0 & \cos\theta \end{bmatrix}.$$

- $\boldsymbol{S}_i$ is the scattering matrix of the target. Here we consider same $\boldsymbol{S}_i$ for both the direct and reflected paths assuming that their angular separation is not large.
- $\boldsymbol{\Gamma}_j = \mathrm{diag}\{\gamma_j^{\mathrm{h}}, \gamma_j^{\mathrm{v}}\}$ denotes the reflection matrix, where

$$\begin{aligned}
\gamma_j^{\mathrm{h}} &\triangleq \frac{\sin\theta_j^{\mathrm{r}} - \sqrt{\epsilon_0 - \cos^2\theta_j^{\mathrm{r}}}}{\sin\theta_j^{\mathrm{r}} + \sqrt{\epsilon_0 - \cos^2\theta_j^{\mathrm{r}}}},\\
\gamma_j^{\mathrm{v}} &\triangleq \frac{\epsilon_0\sin\theta_j^{\mathrm{r}} - \sqrt{\epsilon_0 - \cos^2\theta_j^{\mathrm{r}}}}{\epsilon_0\sin\theta_j^{\mathrm{r}} + \sqrt{\epsilon_0 - \cos^2\theta_j^{\mathrm{r}}}},
\end{aligned}$$

  and ϵ_0 is the relative permittivity at the reflecting surface.
- The transmitting polarization vector is given as

$$\boldsymbol{p}(\alpha_i,\beta_i) \triangleq \begin{bmatrix} \cos\alpha_i & \sin\alpha_i \\ -\sin\alpha_i & \cos\alpha_i \end{bmatrix}\begin{bmatrix} \cos\beta_i \\ j\sin\beta_i \end{bmatrix},$$

  with α and β are the orientation and ellipticity of the polarization ellipse.
- $\boldsymbol{a} \triangleq \left[a_0, a_1, \ldots, a_{L-1}\right]^T$ represents the complex weights transmitted over L transmitters (and also subcarriers).
- The delays and Doppler frequencies are expressed as

$$\begin{aligned}
\tau_{ij}^{\mathrm{dd}} &= \tau(h_i') + \tau\left(h_j'\right), \quad \tau_{ij}^{\mathrm{dr}} = \tau(h_i') + \tau\left(-h_j'\right),\\
\tau_{ij}^{\mathrm{rd}} &= \tau(-h_i') + \tau\left(h_j'\right), \quad \tau_{ij}^{\mathrm{rr}} = \tau(-h_i') + \tau\left(-h_j'\right),\\
f_{\mathrm{D}ij}^{\mathrm{dd}} &= f_{\mathrm{D}}(h_i') + f_{\mathrm{D}}\left(h_j'\right), \quad f_{\mathrm{D}ij}^{\mathrm{dr}} = f_{\mathrm{D}}(h_i') + f_{\mathrm{D}}\left(-h_j'\right),\\
f_{\mathrm{D}ij}^{\mathrm{rd}} &= f_{\mathrm{D}}(-h_i') + f_{\mathrm{D}}\left(h_j'\right), \quad f_{\mathrm{D}ij}^{\mathrm{rr}} = f_{\mathrm{D}}(-h_i') + f_{\mathrm{D}}\left(-h_j'\right),
\end{aligned}$$

  where

$$\begin{aligned}
\tau(h) &\triangleq \frac{1}{c}\left[\sqrt{x^2+y^2+(z'-h)^2}\right],\\
f_{\mathrm{D}}(h) &\triangleq \frac{f_i}{c}\left[\frac{x\dot{x}+y\dot{y}+(z'-h)\dot{z}'}{\sqrt{x^2+y^2+(z'-h)^2}}\right],
\end{aligned}$$

  and $f_i = f_{\mathrm{c}} + i\,\Delta f$ denoting the i-th transmitting frequency.

Stacking the measurements of all $L \times L$ transmitter-receiver pairs and N temporal instants into a $2L^2N \times 1$ column vector we get

$$\boldsymbol{y}(\boldsymbol{x}_k) = \boldsymbol{\mu}(\boldsymbol{x}_k) + \boldsymbol{c} + \boldsymbol{e}, \qquad (12)$$

where $\boldsymbol{y} = [\boldsymbol{y}(t_0), \boldsymbol{y}(t_1), \ldots, \boldsymbol{y}(t_{N-1})]^T$ and $\boldsymbol{y}(t_n) = \left[\boldsymbol{y}_{00}(t_n), \ldots, \boldsymbol{y}_{0L-1}(t_n), \ldots, \boldsymbol{y}_{1L-1}(t_n), \ldots, \boldsymbol{y}_{L-1L-1}(t_n)\right]^T$; similarly for $\boldsymbol{\mu}$, $\boldsymbol{c}$, and $\boldsymbol{e}$.

C. Clutter Model and Statistical Assumptions

In LGA scenarios, it is found that the clutter from the sea surface produces spikes or higher amplitude returns, and therefore its probability density function exhibits heavy tails which is significantly deviated from a standard Gaussian model [20], [21]. Hence, reasoning from the physical mechanism a two-scale sea-surface scattering model, termed compound-Gaussian model, is developed [9], [10]. This model belongs to the class of the spherically invariant random process (SIRP) [22], and has now attained wide acceptance [23]-[26]. According to this model, the complex envelope of the sea-clutter returns can be written as a product of two components

$$\boldsymbol{c}_{ij}(t) = \sqrt{u}\boldsymbol{\chi}(t), \qquad (13)$$

where $\boldsymbol{\chi}(t)$, referred to as speckle, is a fast-changing component that accounts for local backscattering, and u, referred to as texture, is a slow-changing component that describes the underlying mean power level. The speckle component is assumed to be a stationary complex Gaussian process with zero mean and covariance $\boldsymbol{\Sigma}$ and texture component is modeled as an inverse gamma random variable, since this fits well with the real sea-clutter data [27].

We assume that the thermal noise component, $\boldsymbol{e}_{ij}(t)$, is complex Gaussian vector with zero mean and covariance $\sigma_{\mathrm{e}}^2\boldsymbol{I}_2$ and it is uncorrelated with the clutter return. Then, assuming uncorrelatedness among different frequency channels and temporal whiteness, we can write the conditional distribution of the measurement vector as

$$\boldsymbol{y}(\boldsymbol{x}_k)|u,\boldsymbol{\mu}(\boldsymbol{x}_k) \sim \mathbb{C}\mathcal{N}_{2L^2N}\left(\boldsymbol{\mu}(\boldsymbol{x}_k),\, \boldsymbol{I}_{L^2N} \otimes (u\boldsymbol{\Sigma} + \sigma_{\mathrm{e}}^2\boldsymbol{I}_2)\right).$$

IV. Tracking Filter

We employ a sequential Monte Carlo method (particle filter), which is known to be powerful for solving nonlinear and non-Gaussian Bayesian inference problems. In this approach the key idea is to represent the posterior density function by a set of random sample points with associated weights and to compute the required estimates based on these samples and weights.

Let $\boldsymbol{x}_k^{(i)}, i = 1, 2, \ldots, N_{\mathrm{x}}$, denote the sample points with associated weights $w_k^{(i)}, i = 1, 2, \ldots, N_{\mathrm{x}}$, that characterize the posterior density function at the k-th time instant. Mathematically

$$p(\boldsymbol{x}_k|\boldsymbol{y}_k) \approx \sum_{i=1}^{N_{\mathrm{x}}} w_k^{(i)} \delta\left(\boldsymbol{x}_k - \boldsymbol{x}_k^{(i)}\right). \tag{14}$$

However, in practice the samples $\boldsymbol{x}_k^{(i)}, i = 1, 2, \ldots, N_{\mathrm{x}}$, are generated from a proposal (or importance) density function $q\left(\boldsymbol{x}_k^{(i)}|\boldsymbol{x}_{k-1}^{(i)}, \boldsymbol{y}_k\right)$, which is easier to sample from. Then, the corresponding weights are updated as

$$w_k^{(i)} \propto w_{k-1}^{(i)} \frac{p\left(\boldsymbol{y}_k|\boldsymbol{x}_k^{(i)}\right) p\left(\boldsymbol{x}_k^{(i)}|\boldsymbol{x}_{k-1}^{(i)}\right)}{q\left(\boldsymbol{x}_k^{(i)}|\boldsymbol{x}_{k-1}^{(i)}, \boldsymbol{y}_k\right)}. \tag{15}$$

In this work, we use the transitional prior, $p\left(\boldsymbol{x}_k^{(i)}|\boldsymbol{x}_{k-1}^{(i)}\right)$, as the importance density function and the importance weights are realized as $w_k^{(i)} \propto w_{k-1}^{(i)} p\left(\boldsymbol{y}_k|\boldsymbol{x}_k^{(i)}\right)$. However, since our likelihood function does not have a closed-form expression, we use the generalized Gauss-Laguerre quadrature formula [28, Ch. 5.3] to numerically evaluate

$$p(\boldsymbol{y}_k|\boldsymbol{x}_k^{(i)}) = \int_{\mathcal{U}} p(\boldsymbol{y}_k|u, \boldsymbol{x}_k^{(i)}) p(u) du \approx \sum_{g=1}^{G} \widetilde{w}_g \, p(\boldsymbol{y}_k|u_g, \boldsymbol{x}_k^{(i)}),$$

where G is the quadrature order, and u_g and $\widetilde{w}_g$ are the abscissas and weights of the generalized Gauss-Laguerre quadrature.

V. Numerical Results

We present below numerical examples to demonstrate the performance improvement due to the proposed target tracking method. We consider a target that starts at a position $(x, y, z) = (17.32 \text{ km}, 10 \text{ km}, 20 \text{ m})$ and is moving with a velocity of $1000\,(= 1000\cos(\pi/9)\hat{i} + 1000\sin(\pi/9)\hat{j} + 0\hat{k})$ m/s. We assume that the target scattering parameters are partially known ($\vartheta_l = 45°$, $\varepsilon_l = 36°$, $\varrho_l = 0°$, $\nu_l = 0°$, $\gamma_l = 0°$, for $l = 1, \ldots, L$) except for $\boldsymbol{m}$. To track this target we employ an OFDM MIMO radar with the following specifications: carrier frequency $f_{\mathrm{c}} = 1$ GHz; total bandwidth $B = 100$ MHz; number of subcarriers (and transceivers) $L = 3$ (forming a 3×3 co-located MIMO configuration); subcarrier spacing $\Delta f = B/(L+1) = 25$ MHz; positions of the transceivers are $(0, 0, 30)$, $(0, 0, 30.15)$, and $(0, 0, 30.3)$ m; pulse width $T = 1/\Delta f = 40$ ns; pulse repetition interval $T_{\mathrm{PRI}} = 2$ ms; number of temporal samples $N = 5$.

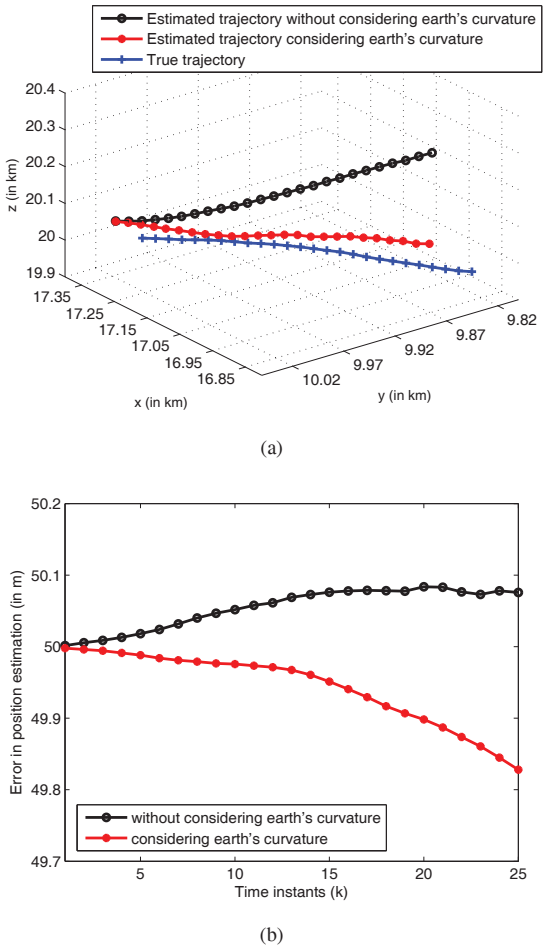

Fig. 3. (a) Comparison of the tracking performances and (b) associated errors in position estimation due to the earth's curvature and standard lower atmosphere modeling.

Fig. 3 depicts the tracking performance and associated errors in position estimation due to the effects of earth's curvature and standard lower atmosphere modeling. It is evident from these plots that we achieve better tracking accuracy by incorporating the underlying physical effects. In Fig. 4 we plot the tracking performance and associated position errors for two MIMO and one single-input-single-output (SISO) configurations. We varied the power per transmitter accordingly to ensure that all of these three configurations transmit the same amount of power per pulse. The results clearly demonstrate the improvement gained due to OFDM MIMO configuration. Though the overall errors in position estimation for the SISO and 2×2 MIMO setups look similar, from Fig. 4(a) we notice that the SISO estimation actually lost the height information of the true trajectory.

VI. Conclusions

We developed a tracking method under the low-grazing angle scenario, incorporating the effects of earth's curvature, vertical refractivity gradient of standard lower atmosphere, and

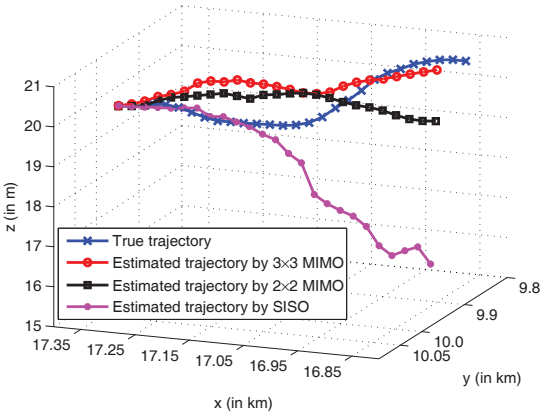

(a)

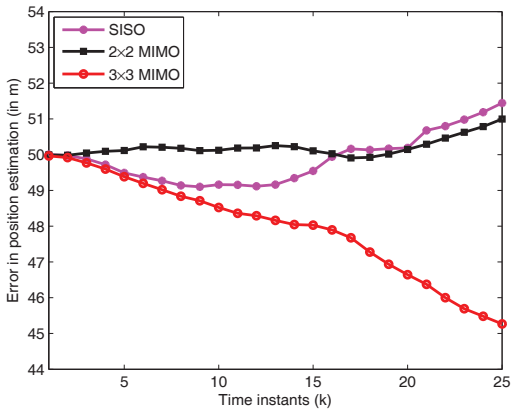

(b)

Fig. 4. (a) Comparison of the tracking performances and (b) associated errors in position estimation due to OFDM MIMO configuration.

non-Gaussian characteristics of sea clutter. We first presented a dynamic state model by considering the target scattering coefficients at different frequencies along with its position and velocity into the state vector. Then, we developed the parametric measurement model of an OFDM MIMO radar system employing polarization-sensitive transceivers. Based on the state and measurement model, we used a sequential Monte Carlo tracker (particle filter). We presented numerical examples to show the effects of realistic physical and statistical modeling and performance improvement achieved due to OFDM MIMO configuration. In our future work, we will consider more realistic physical phenomena, such as multiple order reflections between the transmitter and receiver pairs, signal-dependent clutter returns, etc. We will also extend our work to address the problem of multi-target tracking.

REFERENCES

[1] D. Barton, "Low-angle radar tracking," *Proc. of the IEEE*, vol. 62, no. 6, pp. 687–704, Jun. 1974.

[2] W. White, "Low-angle radar tracking in the presence of multipath," *IEEE Trans. Aerosp. and Electron. Syst.*, vol. AES-10, no. 6, pp. 835–852, Nov. 1974.

[3] A. Mrstik and P. Smith, "Multipath limitations on low-angle radar tracking," *IEEE Trans. Aerosp. and Electron. Syst.*, vol. AES-14, no. 1, pp. 85–102, Jan. 1978.

[4] Y. Bar-Shalom, A. Kumar, W. Blair, and G. Groves, "Tracking low elevation targets in the presence of multipath propagation," *IEEE Trans. Aerosp. and Electron. Syst.*, vol. 30, no. 3, pp. 973–979, Jul. 1994.

[5] J. E. Freehafer, W. T. Fishback, W. H. Furry, and D. E. Kerr, "Theory of propagation in a horizontal stratified atmosphere," in *Propagation of Short Radio Waves*, D. E. Kerr, Ed. NY: McGraw-Hill Book Company, Inc., 1951.

[6] A. Giger, *Low-Angle Microwave Propagation: Physics and Modeling*. Boston, MA: Artech House Publishers, Jul. 1991.

[7] H. Hitney, J. Richter, R. Pappert, K. Anderson, and G. Baumgartner, "Tropospheric radio propagation assessment," *Proc. of the IEEE*, vol. 73, no. 2, pp. 265–283, Feb. 1985.

[8] B. R. Bean and E. J. Dutton, *Radio Meteorology*. New York, NY: Dover Publications, 1968.

[9] J. Wright, "A new model for sea clutter," *IEEE Trans. Antennas Propag.*, vol. 16, no. 2, pp. 217–223, Mar. 1968.

[10] F. Bass, I. Fuks, A. Kalmykov, I. Ostrovsky, and A. Rosenberg, "Very high frequency radiowave scattering by a disturbed sea surface - Part II: Scattering from an actual sea surface," *IEEE Trans. Antennas Propag.*, vol. 16, no. 5, pp. 560–568, Sep. 1968.

[11] T. Lo and J. Litva, "Low-angle tracking using a multifrequency sampled aperture radar," *IEEE Trans. Aerosp. and Electron. Syst.*, vol. 27, no. 5, pp. 797–805, Sep. 1991.

[12] M. A. Sletten, D. B. Trizna, and J. P. Hansen, "Ultrawide-band radar observations of multipath propagation over the sea surface," *IEEE Trans. Antennas Propag.*, vol. 44, no. 5, p. 646, May 1996.

[13] A. Pandharipande, "Principles of OFDM," *IEEE Potentials*, vol. 21, no. 2, pp. 16–19, Apr. 2002.

[14] J. Li and P. Stoica, "MIMO radar with colocated antennas," *IEEE Signal Process. Mag.*, vol. 24, no. 5, pp. 106–114, Sep. 2007.

[15] A. Nehorai and E. Paldi, "Vector-sensor array processing for electromagnetic source localization," *IEEE Trans. Signal Process.*, vol. 42, pp. 376–398, Feb. 1994.

[16] B. Hochwald and A. Nehorai, "Identifiability in array processing models with vector-sensor applications," *IEEE Trans. Signal Process.*, vol. 44, pp. 83–95, Jan. 1996.

[17] T. Lo and J. Litva, "Use of a highly deterministic multipath signal model in low-angle tracking," *IEE Proceedings F - Radar and Signal Proc.*, vol. 138, no. 2, pp. 163–171, Apr. 1991.

[18] J. Huynen, "Measurement of the target scattering matrix," *Proc. of the IEEE*, vol. 53, no. 8, pp. 936–946, Aug. 1965.

[19] D. Giuli, "Polarization diversity in radars," *Proc. of the IEEE*, vol. 74, no. 2, pp. 245–269, Feb. 1986.

[20] A. Farina, F. Gini, M. Greco, and L. Verrazzani, "High resolution sea clutter data: Statistical analysis of recorded live data," *IEE Proc. - Radar, Sonar and Navigation*, vol. 144, no. 3, pp. 121–130, Jun. 1997.

[21] M. Greco, F. Bordoni, and F. Gini, "X-band sea-clutter nonstationarity: Influence of long waves," *IEEE J. Ocean. Eng.*, vol. 29, no. 2, pp. 269–283, Apr. 2004.

[22] E. Conte and M. Longo, "Characterisation of radar clutter as a spherically invariant random process," *IEE Proc. F - Communications, Radar and Signal Proc.*, vol. 134, no. 2, pp. 191–197, Apr. 1987.

[23] K. Ward, C. Baker, and S. Watts, "Maritime surveillance radar. I. Radar scattering from the ocean surface," *IEE Proc. F - Radar and Signal Proc.*, vol. 137, no. 2, pp. 51–62, Apr. 1990.

[24] K. Sangston and K. Gerlach, "Coherent detection of radar targets in a non-Gaussian background," *IEEE Trans. Aerosp. and Electron. Syst.*, vol. 30, no. 2, pp. 330–340, Apr. 1994.

[25] J. Wang, A. Dogandzic, and A. Nehorai, "Maximum likelihood estimation of compound-Gaussian clutter and target parameters," *IEEE Trans. Signal Process.*, vol. 54, no. 10, pp. 3884–3898, Oct. 2006.

[26] S. Sira, D. Cochran, A. Papandreou-Suppappola, D. Morrell, W. Moran, S. Howard, and R. Calderbank, "Adaptive waveform design for improved detection of low-RCS targets in heavy sea clutter," *IEEE Journal of Selected Topics in Signal Proc.*, vol. 1, no. 1, pp. 56–66, Oct. 2007.

[27] A. Balleri, A. Nehorai, and J. Wang, "Maximum likelihood estimation for compound-Gaussian clutter with inverse gamma texture," *IEEE Trans. Aerosp. and Electron. Syst.*, vol. 43, no. 2, pp. 775–779, Apr. 2007.

[28] R. A. Thisted, *Elements of Statistical Computing: Numerical Computation*, 1st ed. New York, NY: Chapman & Hall/CRC, Mar. 1988.